Elucidating dynamics and mechanism of cyclic bioreaction networks using topologically-equivalent electrical circuits

Nath, Sarang S.; Nielsen, Lars K.; Villadsen, John

Published in:
Chemical Engineering Science

Link to article, DOI:
10.1016/j.ces.2022.118015

Publication date:
2022

Document Version
Publisher's PDF, also known as Version of record

Chemical Engineering Science 262 (2022) 118015

Contents lists available at ScienceDirect

Chemical Engineering Science

journal homepage: www.elsevier.com/locate/ces

Elucidating dynamics and mechanism of cyclic bioreaction networks using topologically-equivalent electrical circuits

Sarang S. Nath [a,*], Lars K. Nielsen [a,b], John Villadsen [c,1]

[a] The Novo Nordisk Foundation Center for Biosustainability, Technical University of Denmark, Kgs. Lyngby 2800, Denmark
[b] Australian Institute for Bioengineering and Nanotechnology, The University of Queensland, Brisbane 4072, Australia
[c] Department of Chemical and Biochemical Engineering, Technical University of Denmark, Kgs. Lyngby 2800, Denmark

HIGHLIGHTS

- A novel method is developed to convert biochemical reaction networks into electrical circuit analogs.
- The electrical analog is then simulated to yield bioreaction network dynamics.
- Application of the model is shown to quantify the dynamics of the dihydrofolate reductase pathway.
- The method is modular and works with linear and nonlinear reaction rate laws.
- The graph reveals network topology and is suitable for integration with other bioreaction models.

GRAPHICAL ABSTRACT

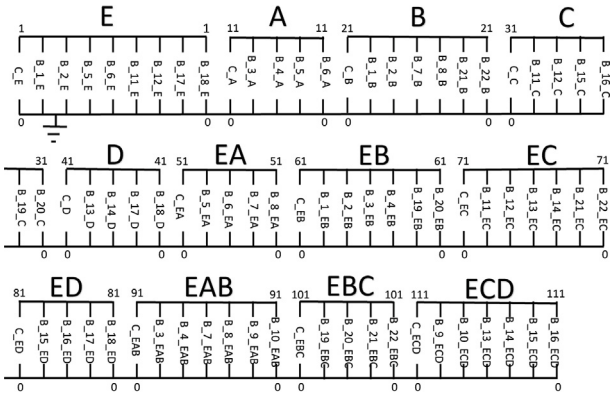

ARTICLE INFO

Article history:
Received 16 June 2022
Received in revised form 5 August 2022
Accepted 15 August 2022
Available online 19 August 2022

Keywords:
Biochemical reaction networks
Bionetworks
Electrical analogs
Dihydrofolate reductase
Network dynamics
Molecular mechanism
Kinetic analysis
Maximum flux
Steady-state rate
Cycles and sub-cycles
Electrical circuits
Graph theory

ABSTRACT

A novel methodology is established to convert a set of elementary chemical reactions into topologically-equivalent electrical circuits. The circuit analog is then simulated to elucidate the dynamics of complex cyclic bionetworks. The pyramidal reaction network catalyzed by the universal enzyme dihydrofolate reductase – which has important pharmacological and medical relevance in connection with cancer therapy – is used to illustrate the application of our model. The finite number of mechanisms, sub-cycles, or graphs constituting the cyclic network are analyzed, their contribution to the overall steady-state reaction rate determined, and the most probable mechanism is identified. The developed methodology is elegant, modular, and permits representation and visualization of network structure and topology at a glance. It can handle linear and nonlinear kinetics/rate laws, does not require simplifying assumptions such as use of the quasi-steady-state/Bodenstein approximation or the absence of nonlinear kinetic steps in the intermediates, and is suitable for coupling and integration with other flux-based reaction models.

* Corresponding author.
E-mail addresses: nathsarang@gmail.com, sasuna@biosustain.dtu.dk (S.S. Nath).
[1] Deceased July 22, 2021.

https://doi.org/10.1016/j.ces.2022.118015
0009-2509/

1. Introduction

Chemical reactions in biological systems generate complex pathways and networks, and there has been a constant search for novel and improved methods that can quantify their kinetics and elucidate network dynamics and mechanism (Hill, 1989; Helfferich, 2001; Bak et al., 2002; Fishtik et al., 2004; Murzin and Avetisov, 2007; Hardiman et al., 2009; Beezer and Hansen, 2012; Karlsson et al., 2010; Huang et al., 2017; Juretić et al., 2019; Pellissier–Tanon et al., 2021; Chouket et al., 2022). King and Altman (1956) had first proposed a graphical method to write down rate laws for enzyme-catalyzed reactions. While the method worked well for single-cycle networks, the algorithm was not readily implementable for branched systems, or complex multi-cycle pathways and cyclic networks. Hill (1989) and Poland (1989) extended the method to deal with cyclic systems and determine the steady-state rates in more complex enzymatic reactions. However, they required several simplifying approximations, did not determine network dynamics, and the appropriate diagrams had to be drawn by inspection. These methods could not readily ensure complete identification of the large number of constituent subsystems or sub-cycles in complex networks in order to correctly evaluate the steady-state reaction rates.

Subsequently, Happel and Sellers (1992), Helfferich (2001), and Chen and Chern (2003) presented improved methodologies based on the Bodenstein approximation or other linearized approaches to find general rate equations for complex reaction networks. The fundamental assumption made in these studies for treatment of three-dimensional topological networks was that there the kinetics contain no nonlinear steps in the intermediates. This prevented application of the methods to cyclic reaction networks containing three or more intersecting reaction pathways that followed second-order or nonlinear kinetics.

Cellier (1991) and Wiechert (2002) surveyed various kinetic models and found that the predictive power of the models is "not very high" and considered the transfer of modeling methodology from chemical to biological processes a "very ambitious task." Wiechert (2002) predicted that it is unlikely that quantitatively predictive models with a broad scope will be obtained. The workers suggested that electrical circuits be used in the modeling since they have much in common with chemical reaction networks. Fishtik et al. (2004) developed a powerful theory and algorithm for reaction routes using electrical analogs. Mandal and Sarpeshkar (2009) also exploited analogies between electronics and chemistry and developed log-domain circuit analogs for some simple chemical reactions using field-effect transistors. There are several differences between these approaches and the method adopted in this work. For instance, Mandal and Sarpeshkar (2009) require several *types* of electrical elements, i.e. capacitors, transistors, integrators, and current mirrors in their circuits, while we use only capacitors and nonlinear current sources. The *number* of electrical elements of a particular type required to model even a simple bimolecular reaction (their Fig. 2) in their approach is many-fold greater than that needed in our implementation (Section 4). Mandal and Sarpeshkar (2009) also need to fix the values of several additional parameters (their β_1, β_2, and fixed current I_{min}) in their protocols, none of which are necessary in our implementation (Sections 2–4). They do not model complex bioreaction networks such as those carried out in this work (Section 5). Finally there are speed advantages in our simulations compared to simulations of previous approaches. Furthermore, several differences were also identified between electrical and biological networks, and these differences (Section 2) precluded the analogy between the two from being developed and exploited by researchers.

In this work, we have attempted to fill the above gaps in knowledge and have developed a broad and novel methodology that converts chemical reaction networks to electrical analogs (Section 2.1). We have shown topological equivalence between the chemical and electrical systems using Kirchhoff's laws (Section 2.2). In Sections 3–5 we simulate the dynamics first of simple networks, and then apply the methodology to a fairly complex, pyramidal biological network of reactions involving dihydrofolate reductase (Section 5), and offer novel insights into the mechanism of catalysis.

Dihydrofolate reductase (EC 1.5.1.3) is a universal enzyme that catalyzes the NADPH-dependent reduction of 7,8-dihydrofolate (H_2F) to 5,6,7,8-tetrahydrofolate (H_4F). It is responsible for maintaining intracellular pools of H_4F, a task of great clinical importance, because H_4F is the cofactor used in synthesis of several important metabolites (Blakley, 1969). One of these metabolites is thymidylate, a key building block of DNA. The enzyme is well-recognized as a drug target for inhibiting DNA synthesis in cancer cells. Increase in dihydrofolate reductase levels caused by treatment with the anti-tumor agent methotrexate during chemotherapy is one of the key mechanisms of resistance to this drug. Hence it is important to develop rapid experimental and computational methods that can follow the time evolution of the concentration of dihydrofolate reductase and other intermediates in the dihydrofolate pathway. The many important pharmacological applications of dihydrofolate reductase have been cogently described by Hitchings (1989) in his Nobel lecture.

Given the importance of the dihydrofolate reductase pathway mentioned above, several experimental characterization studies of the enzyme from various sources, such as *Escherichia coli* (Fierke et al., 1987), *Thermotoga maritima* (Loveridge et al., 2017) and *Mycobacterium tuberculosis* (Czekster et al., 2011) are available in the biochemical literature. Studies in physical chemistry have tried to model its kinetics, mainly by enhanced King-Altman methods originally published in the physical chemistry literature (King and Altman, 1956; Poland, 1989; Happel and Sellers, 1992; Juretić et al., 2019; Pellissier–Tanon et al., 2021). Chemical engineering researchers have also attempted to quantify the steady-state kinetics of dihydrofolate reductase (Helfferich, 2001; Chen and Chern, 2003; Fishtik et al., 2004) and check for thermodynamic consistency of the determined kinetic parameters (Murzin and Avetisov, 2007). However, we were unable to locate such reports in the biochemical engineering literature, although the importance of these studies has been repeatedly pointed out in the context of metabolic systems (Wiechert, 2002; Hardiman et al., 2009; Karlsson et al., 2010).

Given the above, we have attempted to develop in considerable detail the dynamics of the dihydrofolate reductase pathway by our equivalent electrical circuit methodology. We have also tried to elucidate the most probable mechanism of the wild-type *Escherichia coli* enzyme from the kinetic analysis by reduction of the possible cyclic sub-pathways, and by determining the contribution of the various sub-cycles to the net overall steady-state reaction rate of the network (Section 5).

2. Methods

2.1. Basic approach

Elementary unimolecular irreversible reactions involving two chemical species are selected to illustrate our novel approach, and establish topological equivalence between the chemical and electrical representations. The electrical circuit approach is subsequently extended to linear and nonlinear cyclic reaction networks in Section 3.

The reaction networks are simulated by modeling each species as a capacitor (C_A and C_B in Fig. 1) with a capacity of 1 Farad. The initial voltage across the capacitor is set to represent the initial concentration of the corresponding species (100 V for a reactant and 0 V for all intermediates and products). Each reaction is modeled by allowing a resistor to drain a current from the reacting species capacitor to ground. This resistor (R_AB in Fig. 1) has a value of resistance that is inversely proportional to the rate constant of the reaction. A zero volt dummy voltage source (V_AB in Fig. 1) is connected in series with this resistor to measure the current through this branch of the circuit. The current flowing through the resistor models the consumption of a particular reactant. To model the production of the product, the *same* current is made to flow into the product capacitor using a current-controlled current source (F_AB; see Fig. 1). The dynamics of the system is studied by using the established electrical simulation software SPICE (Roberts and Sedra, 2010) that uses damped Newton-Raphson (sparse) matrix algorithms to solve circuits with nonlinear components. This approach is similar to that taken by other standard differential equation solver packages; for a succinct explanation of the inner workings of SPICE, see Warwick (2009). From the obtained solution, the variation of the voltage is plotted across the species capacitors as a function of time. The output plot of the concentration profile i.e., exponential decrease in A and exponential increase in B, matches the results obtained by standard differential equation methods in chemical kinetics (Levenspiel, 2006).

The above methodology for generation of the electrical analog was required to surmount the difficulties that were encountered previously in converting chemical reaction networks to equivalent electrical circuits (Cellier, 1991; Wiechert, 2002). In our view, these difficulties fundamentally arise from intrinsic differences in structure between potential and kinetic theory, which were not emphasized in the previous works. In the former class of theories, the current was represented as being proportional to a difference in potential between any two points A and B on a potential energy surface, in accordance with numerous experimental findings. However, for a chemical reaction $A \xrightarrow{k_1} B$, the reaction rate is found to be proportional to the concentration, C_A of the reactant and not to a difference in concentration $(C_A - C_B)$. Similarly, for the reverse reaction $B \xrightarrow{k_{-1}} A$ the reaction rate is proportional to the concentration, C_B. Moreover, reversing the concentrations does not yield a rate that is simply equal to and negative of the rate measured before the reversal, unlike in a potential flow.

2.2. Dynamical topological equivalence between electrical and chemical representations

We first establish the dynamical topological equivalence between our electrical circuit representation and the standard chemical formulation based on application of Kirchhoff's laws. We consider the simple irreversible reaction $A \xrightarrow{k} B$ and the circuit shown in Fig. 1.

For a first-order reaction, in the standard chemical model, we have

$$\frac{d[A]}{dt} = -k[A], \frac{d[B]}{dt} = k[A] \tag{1}$$

where k is the rate constant of the reaction and $[A]$ and $[B]$ denote the concentrations of species A and B at any time t. Solving this for the case $[A](t = 0) = [A]_0$ and $[B](t = 0) = 0$ yields the well-known result,

$$[A] = [A]_0 \exp(-kt), [B] = [A]_0\{1 - \exp(-kt)\} \tag{2}$$

For the electrical circuit in Fig. 1, applying Kirchhoff's Loop Law leads to

$$\frac{q}{C_A} + R_{AB}\frac{dq}{dt} + V_{AB} = 0 \tag{3}$$

where q denotes the charge on the capacitor C_A. If there is no external input, $V_{AB} = 0$ and we obtain

$$R_{AB}\frac{dq}{dt} = -\frac{q}{C_A} \Rightarrow C_A R_{AB}\frac{dV_A}{dt} = -V_A \tag{4}$$

where V_A is the voltage drop across C_A. If the capacitances are set to 1 Farad, we have

$$\frac{dV_A}{dt} = -\frac{V_A}{R_{AB}} \Rightarrow V_A = V_A(t = 0)\exp\left(-\frac{t}{R_{AB}}\right) \tag{5}$$

which is identical to the form obtained when applying the law of mass action on the chemical reaction itself. Now, because of the current source in the second loop, we stipulate the currents in both

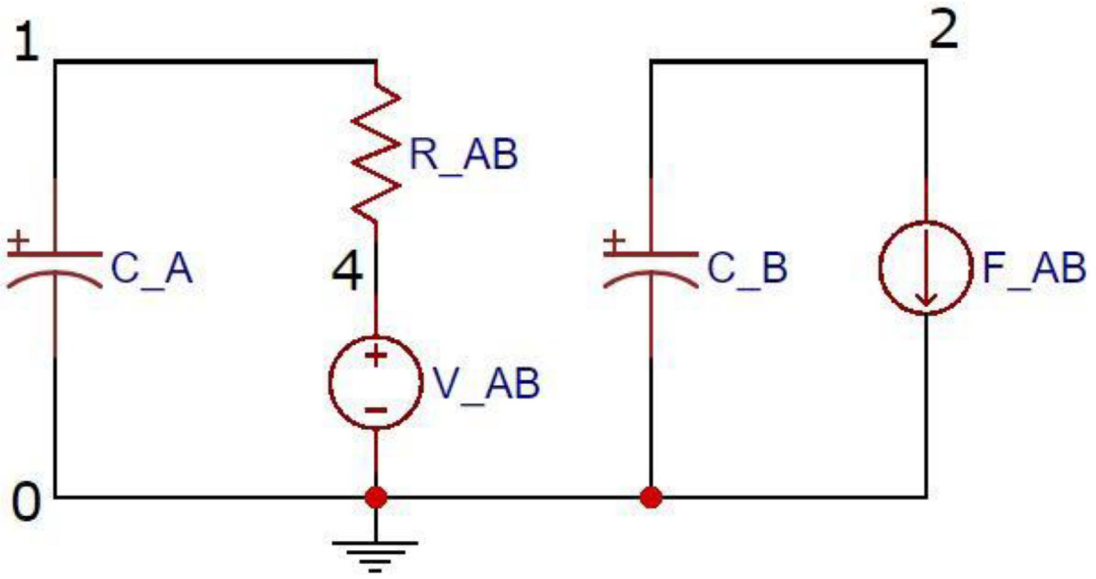

Fig. 1. Equivalent electrical circuit for the irreversible reaction $A \xrightarrow{k} B$. R and C represent a resistor and capacitor respectively, V represents a voltage source, and F represents a current-controlled current source. The resistance R_AB is inversely proportional to the rate constant k and the current in the two loops of the circuit is made equal using F_AB.

loops to be identical. Hence the potential drop across capacitor C_B works out to be

$$V_B = \frac{q}{C_B} = V_A(t=0)\left\{1 - exp\left(-\frac{t}{R_{AB}}\right)\right\} \quad (6)$$

The above results, given by Equation (5) and Equation (6), are identical to those of the chemical version (Equation (2)), and establish dynamical topological equivalence between the electrical and chemical representations, i.e. the dynamics of the electrical and chemical state variables are identical. Similar methods can be applied to different chemical reaction systems of increasing complexity. How far the analogy between the two representations translates into *network* topological equivalence requires a more complex mathematical treatment and is an interesting subject for further research.

3. Dynamics of cyclic systems of unimolecular reactions by the equivalent circuit approach

In order to demonstrate the essential ideas of equivalence between chemical and electrical representations given in Section 2, we first use simple cyclic chemical reactions as examples. We consider the simplest cyclic, unimolecular reaction network with three states, the so-called triangular reaction network, shown in Fig. 2. However, it is not that this simple network is an abstraction, because several chemical and biochemical reaction networks of this type are known. Chemical examples include the isomerization of hexanes over a zeolite catalyst and the isomerization of butenes on alumina catalyst (Huang et al., 2017). An important biological example of the triangular reaction network is the hydrolysis of β-lactams catalysed by β-lactamases (Juretić et al., 2019).

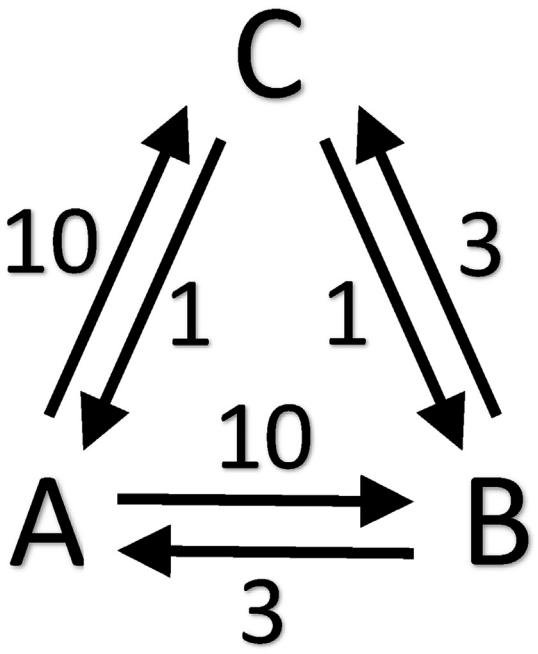

Fig. 2. The three-state triangular reaction network with the forward and backward reaction rate constants (in s^{-1}) specified for hexane isomerization using a zeolite catalyst.

The equivalent electrical circuit for a triangular network of reversible chemical reactions consisting of three species A, B, and C, interconverting into each other is constructed in a modular way and is shown in Fig. 3. The system is modeled by allowing the capacitor C_A to discharge through the resistor R_AB representing the chemical reaction A → B. A zero volt voltage source is attached in the same branch as this resistor, in order to measure the current flow through this resistor. This current flow is reproduced by the current-controlled current source (CCCS) F_AB, and is allowed to flow into C_B. For the reaction B → C, a resistor R_BC is connected in parallel to C_B, and again a zero volt voltage source is connected to this resistor in series. Another CCCS, F_BC is used to reproduce this electrical current, and to feed it into C_C. The modular process is repeated for the reaction A → C. Similarly, an equivalent set of elements is added for the reverse reactions B → A, C → B, and C → A (Fig. 3).

As described above, the triangular reaction network of Fig. 3 involves two incoming and two outgoing reactions from each of the three species. Thus, for each specie-representing capacitor, the circuit analog contains two sets of resistor-zero volt source pair, and two sets of current-controlled current sources (Fig. 3). In the absence of external flux injection or clamping of concentration of terminal species, i.e. for a closed system, the principle of microscopic reversibility places additional constraints. Thus, to make the cycle physically realizable, the rate constants must satisfy detailed balance, also sometimes called the thermodynamic box in the chemical literature. Therefore, in electrical terms, the values of the resistances, which stand for the rate constants, must satisfy the following relationship:

$$R\_AB \times R\_BC \times R\_CA = R\_AC \times R\_CB \times R\_BA \quad (7)$$

The modeling in Fig. 3 exemplifies our modular approach that follows from the elementary building blocks (Fig. 1). The SPICE simulation of the dynamics of this network is illustrated in Fig. 4. The system rapidly reaches steady state, and the steady state concentrations can be readily determined from Fig. 4.

4. Dynamics of bimolecular chemical reactions

Bimolecular and other nonlinear reaction networks are ubiquitous in chemical and biological systems. However they present unique problems while modeling them as equivalent electrical circuits that have not been resolved previously. The flux of the reaction in this case is dependent on more than one voltage, and this

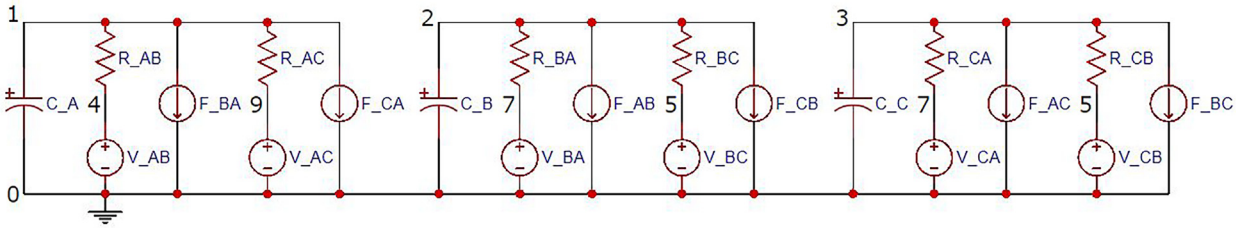

Fig. 3. Equivalent electrical circuit for a reversible triangular reaction cycle, consisting of three species A, B, and C, interconverting into each other. R and C represent a resistor and capacitor respectively, V represents a voltage source, and F represents a current-controlled current source. Numerals represent node numbers. Section 3 contains a detailed description of the various circuit elements.

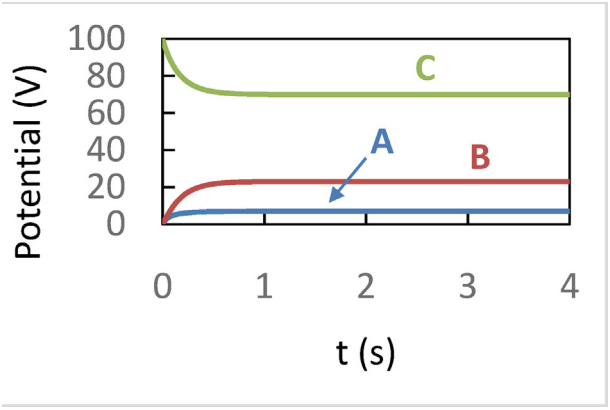

Fig. 4. Computer simulation of the dynamics of the triangular reaction network of Fig. 1 using the topologically-equivalent electrical circuit shown in Fig. 2.

dependence is generally expressed as a product in chemical kinetics. The standard resistor which was used to model unimolecular reactions is no longer adequate for such bimolecular, autocatalytic, and nonlinear systems because the current flowing through the resistor can depend on only one voltage difference, that too in a linear way. The problem is solved here by using a new device, the nonlinear current source (NLCS). This device models a *nonlinear* resistor, and its current characteristics can be set to any mathematical function of the voltages and/or currents in the electrical circuit. For the purpose of these simulations, the current characteristics are defined to be governed by the rate laws for the particular chemical reactions, written in terms of voltages instead of concentrations.

Sets of bimolecular elementary reactions illustrate the above point. The sets are:

$$A + B \xrightarrow{k_1} C$$

$$A + B \xrightarrow{k_1} C + D$$

$$A + B \underset{k_{-1}}{\overset{k_1}{\rightleftharpoons}} C + D \tag{8}$$

Species in reactions (i) to (iii) are modeled as capacitors of capacity 1 Farad each, while the bimolecular chemical reaction is modeled by using sets of NLCSs as discussed above. For instance, in the case of reaction (iii) above, two NLCSs are used to remove an electric current equal to $I(V) = k_1V(A)V(B)$ from both capacitors A and B. Two more NLCSs are used to feed this same current into capacitors C and D. For the reverse reaction, which is also bimolecular, two NLCSs remove a current $I(V) = k_{-1}V(C)V(D)$ from capacitors C and D, and two more are used to feed this current into capacitors A and B.

A shorthand notation with B representing the nonlinear current source, NLCS is employed. This is especially convenient for use in large cyclic reaction networks, such as the dihydrofolate reaction pathway (Section 5). The analogy between components constituting electrical and chemical reaction networks is summarized in Table 1.

Table 1
Analogy between model component elements of electrical and chemical reaction networks.

Chemical reaction network	Electrical network
Chemical species (nodes)	Terminals of electrical elements (nodes)
Elementary chemical reactions (connections)	Electrical elements (connections)
Concentration of chemical species, C	Voltage across capacitor, V
Consumption/production of species	Current flow through resistor or conductor, I
Value of reaction rate constant, k	Value of conductance, κ or inverse of resistance, R
Rates of reaction (linear systems)	Current-controlled current source (CCCS), F
Rates of reaction (nonlinear systems)	Nonlinear current source (NLCS), B

5. Modeling the dihydrofolate reaction network

As an example illustrating the application of our methodology of equivalent electrical circuits to cyclic bioreaction networks, we consider the set of enzymatic reactions involving dihydrofolate reductase. Dihydrofolate reductase is a biologically universal enzyme that catalyzes the NADPH-dependent reduction of 7,8-dihydrofolate (H_2F) to 5,6,7,8-tetrahydrofolate (H_4F). The enzyme is essential for maintaining intracellular levels of H_4F and its derivatives for the biosynthesis of purines, amino acids, and other important metabolites (Blakley, 1969). In addition, it has enormous medical and pharmacological importance, as discussed by Hitchings (1989) in his Nobel lecture, and is the target enzyme for antifolate compounds, such as the anti-cancer drug methotrexate.

An important advance was the elucidation of the entire pathway of wild type *Escherichia coli* dihydrofolate reductase by deriving its pre-steady-state and steady-state kinetics by fast stopped-flow fluorescence experiments (Fierke et al., 1987). The overall reaction is given by

$$H_2F + NADPH \xrightarrow{H^+} H_4F + NADP^+ \tag{9}$$

The rate constants for the 22 reactions of the *Escherichia coli* dihydrofolate reductase reaction network at 25 °C are tabulated in Table 2 (Fierke et al., 1987; Benkovic et al., 1988). These parameters are based on extensive time-resolved stopped flow fluorescence measurements of dihydrofolate reductase kinetics at pH values of 6.0, 6.5, and 9.0, and were reported as pH-independent rate constants by Fierke et al. (1987). Several reaction rate con-

Table 2
Rate constants for the *Escherichia coli* dihydrofolate reaction network (Fierke et al., 1987; Benkovic et al., 1988) at 25 °C. First-order rate constants are in s^{-1}; Pseudo first-order rate constants are given in $\mu M^{-1}\ s^{-1}$.

Reaction number	Elementary reaction	Rate constant
1	E + B → EB	20[B]
2	EB → E + B	3.5
3	EB + A → EAB	40[A]
4	EAB → EB + A	40
5	E + A → EA	40[A]
6	EA → E + A	20
7	EA + B → EAB	5[B]
8	EAB → EA + B	1.7
9	EAB → ECD	950
10	ECD → EAB	0.6
11	EC → E + C	1.4
12	E + C → EC	25[C]
13	ECD → EC + D	200
14	EC + D → ECD	5[D]
15	ECD → ED + C	2.4
16	ED + C → ECD	25[C]
17	ED → D + E	300
18	D + E → ED	13[D]
19	EB + C → EBC	2C
20	EBC → EB + C	12.5
21	EC + B → EBC	8[B]
22	EBC → EC + B	85

stants that describe second order reactions involve species concentrations within brackets (Table 2). Rates that involve the nonlinear product of an intermediate and a terminal species were modeled as first order using pseudo-rate constants with respect to the concentration of the terminal species by researchers subsequently (Poland, 1989; Happel and Sellers 1992; Chen and Chern, 2003). In this way, all the elementary reactions were made first-order with respect to intermediates (Table 2). The basis for this lies in the assumption that the terminal species are expected to be present at far higher concentrations than the concentrations of the intermediates. However, no independent verification of this assumption was made, given the lack of a general technique of testing. Our circuit approach is quite general and can elucidate network dynamics without any requirement of such assumptions, if the second-order or nonlinear rate constants are employed. However, if pseudo-first-order rate constants are reported (Table 1), we can nonetheless use our approach to follow the time evolution of the species and test the validity of the assumptions.

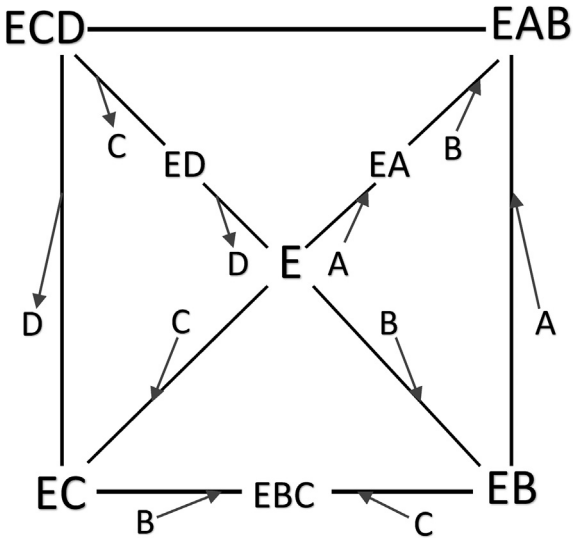

Fig. 5. Biochemical reaction network for the four-node pyramidal dihydrofolate system of reactions. The enzyme dihydrofolate reductase catalyzes the conversion of 7,8-dihydrofolate (H_2F) and NADPH in the presence of H^+ to 5,6,7,8-tetrahydrofolate (H_4F) and $NADP^+$. The overall reaction is given by $H_2F + NADPH \overset{E,H^+}{\rightarrow} H_4F + NADP^+$. In the notation used to represent the reaction network, $A = H_2F$, $B = NADPH$, $C = H_4F$, $D = NADP^+$, and $E =$ dihydrofolate reductase.

Fig. 5 shows the reaction network using the notation $A = H_2F$, $B = NADPH$, $C = H_4F$, $D = NADP^+$, and $E =$ dihydrofolate reductase. The cyclic network can be sub-classified as a pyramidal network with four nodes at the base of the pyramid (Koutrouli et al., 2020). The topologically-equivalent electrical network for the 22 reactions of the dihydrofolate reductase system is shown in Fig. 6. The construction of the equivalent circuit is modular, with a distinct node numbering for each module with a capacitor C representing either a terminal species $A = H_2F$, $B = NADPH$, $C = H_4F$, $D = NADP^+$, or an intermediate species among $E, EA, EB, EC, ED, EAB, EBC, ECD$ (Fig. 6). The interconnections are denoted using various NLCSs, or B-elements in the network that model the various chemical reactions in which the respective chemical species participate. A major advantage of our electrical analog method using the B-elements is their generality, given that they can be used to model reactions with a nonlinear rate law, or reactions with a linearized rate equation, as when pseudo-first-

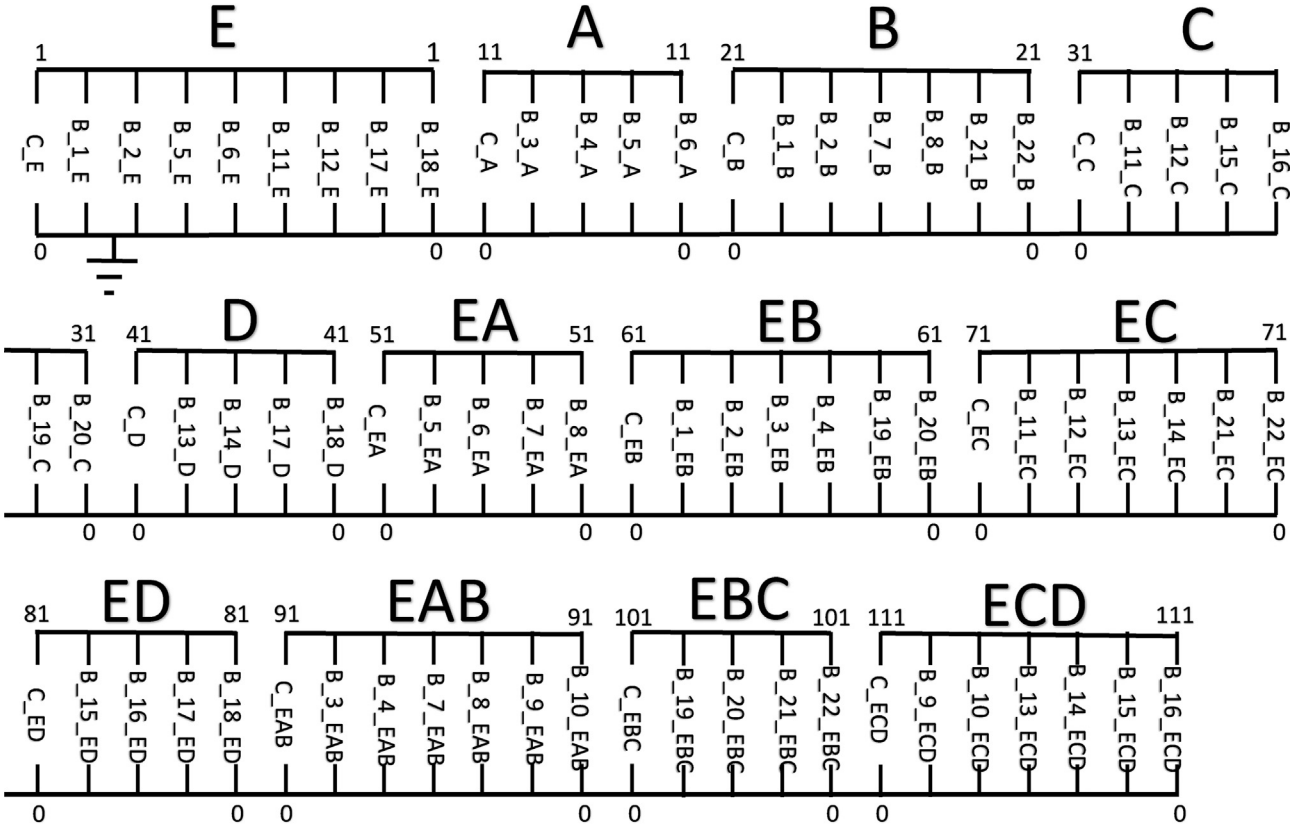

Fig. 6. Equivalent electrical network in shorthand notation for representation of the dihydrofolate reductase system of reactions shown in Fig. 4. C stands for a capacitor, while B represents a nonlinear current source. Numerals represents the reaction number as given in Table 2, and letters represent the reaction species or intermediates.

order rate constants are used. By contrast, the King-Altman-Hill diagram method (King and Altman, 1956; Hill, 1989; Poland, 1989), the method of matrix solution (Happel and Sellers, 1992), and other developed methods such as that of generalized rate equations (Chen and Chern, 2003), use linearized approximations and require that the rate of the forward and reverse elementary reactions be expressed as linear functions of the concentrations of the intermediate species.

The above discussion has shown that the circuit representation (Fig. 6) enables us to *visualize at a glance* the various interconnections in the complex network, and also shows us how the various interaction effects can be modeled and simulated. Another attractive property of the constructed network is its modular nature. If a newly-detected reaction intermediate or a newly-discovered chemical reaction is added to the system of equations of Table 2, we only need to incorporate the new intermediate by a C-element, and the new reaction(s) by additional B-elements in the respective block or module, *without alterations in the existing network structure of the system*. The benefits of modularity and the capability to model nonlinear systems are applicable to the other reaction networks that we have studied (Nath et al., 2021; Nath and Villadsen, 2022; Nath, 2022) and also to Hammerstein-Wiener–type nonlinear networks, where a nonlinear block precedes or follows a linear block, and the nonlinear system can be represented in a modular block diagram form. Generalization to strongly nonlinear dynamical systems and chaos processes of such modular representation and reduction to a block diagram form requires further study. The electrical network shown in Fig. 6 was simulated using the electrical simulation software SPICE (Roberts and Sedra, 2010) for the initial conditions $[A]$ = 0.9 μM, $[B]$ = 0.9 μM, $[C]$ = 0.1 μM, $[D]$ = 0.1 μM, $[E]$ = 1.0 μM. This choice of initial conditions was employed to enable comparison of the reaction rates in our simulation with the steady-state reaction rates of the overall reaction calculated by other methods. The results for the dynamics of the dihydrofolate reductase system are shown in Fig. 7. The concentrations of *A* and *B* decrease (and the concentrations of the products *C* and *D* increase) at a rapid rate initially of $\sim$ 20 μM s^{-1} and settle down to reach a constant steady-state overall reaction rate of 1.70 μM s^{-1}. The results for the steady-state reaction rate of the dihydrofolate reductase pathway computed using the various methods are compared in Table 3. The significant difference between the calculated reaction rates from the simulation (Fig. 7) and the diagram method (Poland, 1989) probably arise from incomplete consideration of all possible reaction pathways by the latter. Diagram methods do not guarantee that all possible pathways that contribute to the overall steady-state reaction rate and flux have been considered, and are therefore not easily adapted to model complex biological networks.

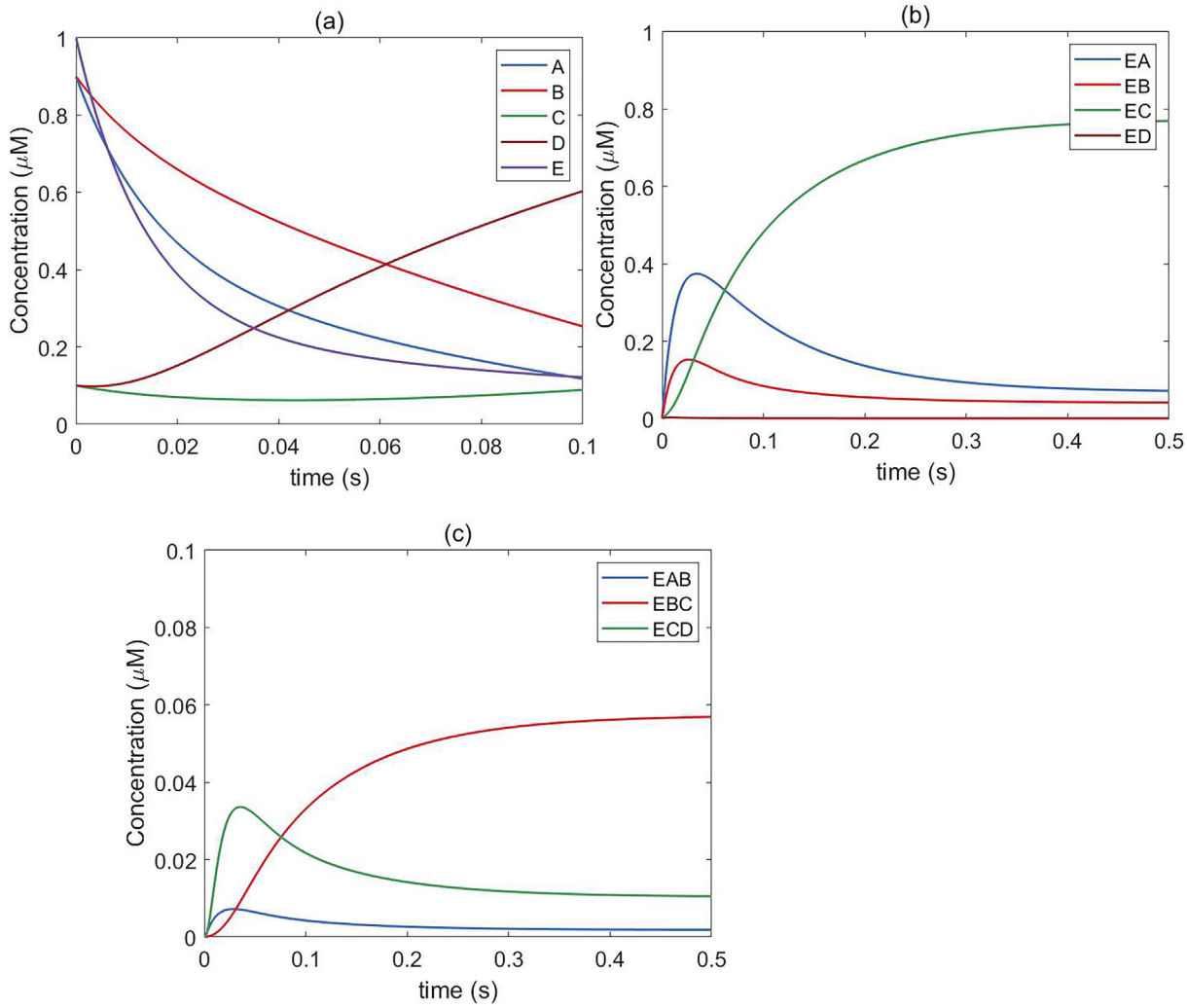

Fig. 7. Computer simulation of the electrical network of Fig. 6 using SPICE to illustrate the dynamics of the dihydrofolate reaction network. Time evolution of the concentrations of *A*, *B*, *C*, *D*, *E* (a); *EA*, *EB*, *EC*, *ED* (b); *EAB*, *EBC*, *ECD* (c). The initial conditions used were: $[A]$ = 0.9 μM, $[B]$ = 0.9 μM, $[C]$ = 0.1 μM, $[D]$ = 0.1 μM, $[E]$ = 1.0 μM.

Table 3
Comparison of calculated overall reaction rates for the *Escherichia coli* dihydrofolate reaction network.

Method of calculation	Steady state reaction rate ($\mu M\ s^{-1}$)	Initial reaction rate ($\mu M\ s^{-1}$)
King-Altman-Hill diagram method [Hill (1989); Poland (1989)]	1.119	Only *steady-state* reaction rates
Matrix method [Happel and Sellers (1992)]	1.697	of *linear* first-order or pseudo-
General rate equation method [Chen and Chern (2003)]	1.702	first-order mass action
		systems can be calculated
		by these methods
Topologically-equivalent electrical circuit method [this work]	1.700	20.0

The state-state concentrations of all reaction intermediates with the exception of the tetrahydrofolate binary complex, [*EC*] are small in comparison to the initial and final concentrations of the reactants and terminal species respectively (Fig. 7), partially justifying the assumptions made in earlier analyses. These assumptions had not been subjected previously to rigorous testing. Among other limitations of these methods (Table 3) is their ability to calculate only the steady-state concentrations and the steady-state reaction rate, and to model linearized systems only. On the other hand, our electrical circuit approach is applicable whether the rate laws used for the elementary forward and reverse reactions are linear, pseudo-linear, or nonlinear, and above all, it yields the system dynamics with its time evolution to the steady-state, and therefore gives greater information on the complex reaction network. At the very least, it enables us to test the extent to which the assumptions of previous analyses are valid.

Some limitations of diagram methods have been pointed out above. The essence of the approach lies in evaluating the product of rate constants divided by the sum of product of rate constants obtained from appropriate diagrams. For the dihydrofolate reductase system (Fig. 5 and Table 2), this amounts to drawing 152 diagrams for the numerator corresponding to each of the eight intermediates in Fig. 5, and $152 \times 8 = 1216$ diagrams for the denominator. The drawing of such a large number of diagrams is practically almost impossible for large networks. Further, each of the 152 terms in the numerator and 1216 terms in the denominator has to be carefully evaluated from the corresponding diagrams. Even if these diagrams are replaced by algebraic expressions, stored as strings of integers in a matrix, and evaluated by a computer, it is still a fairly cumbersome method. However, an improved approach is possible. One can identify the *small* finite set of constituent sub-cycles within the cyclic network (Fig. 5)

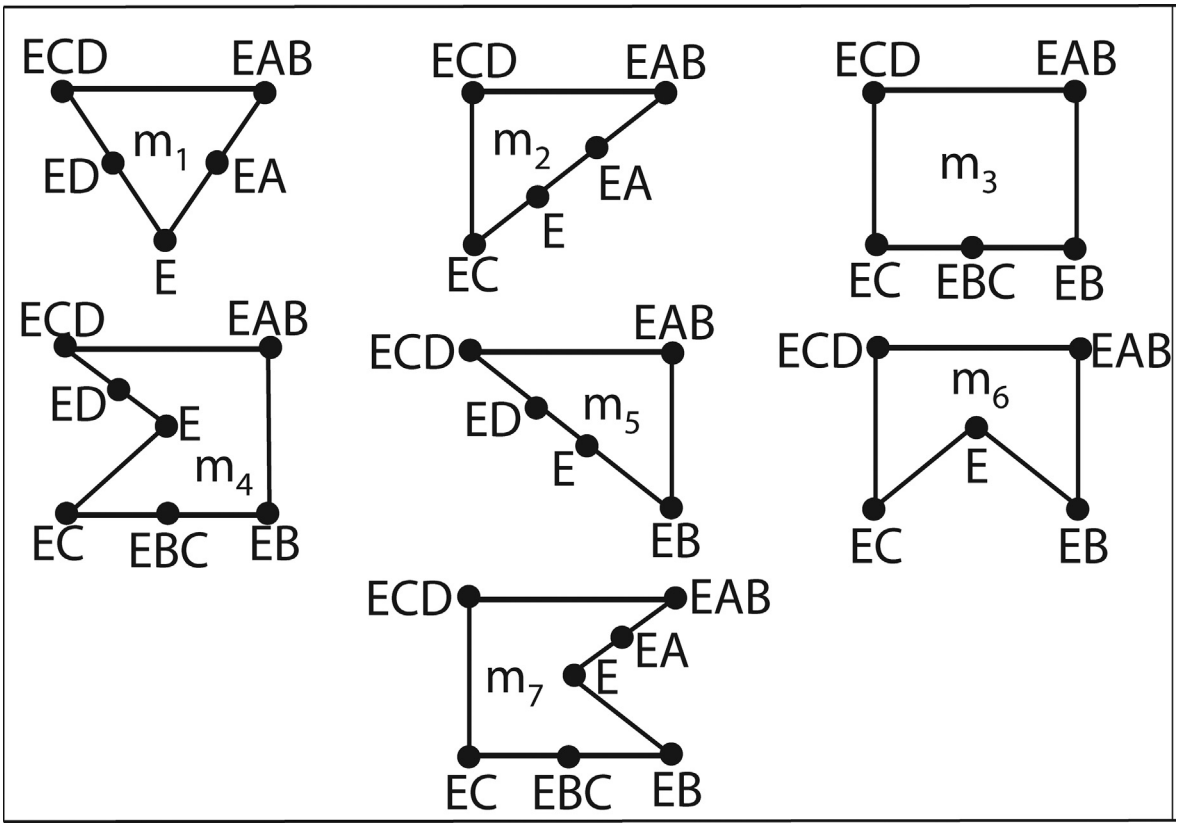

Fig. 8. Network illustration of the seven sub-cycles/mechanisms m_1 to m_7 that result in a net positive steady-state reaction rate for the overall reaction $A + B \overset{E,H^+}{\rightarrow} C + D$ catalyzed by dihydrofolate reductase.

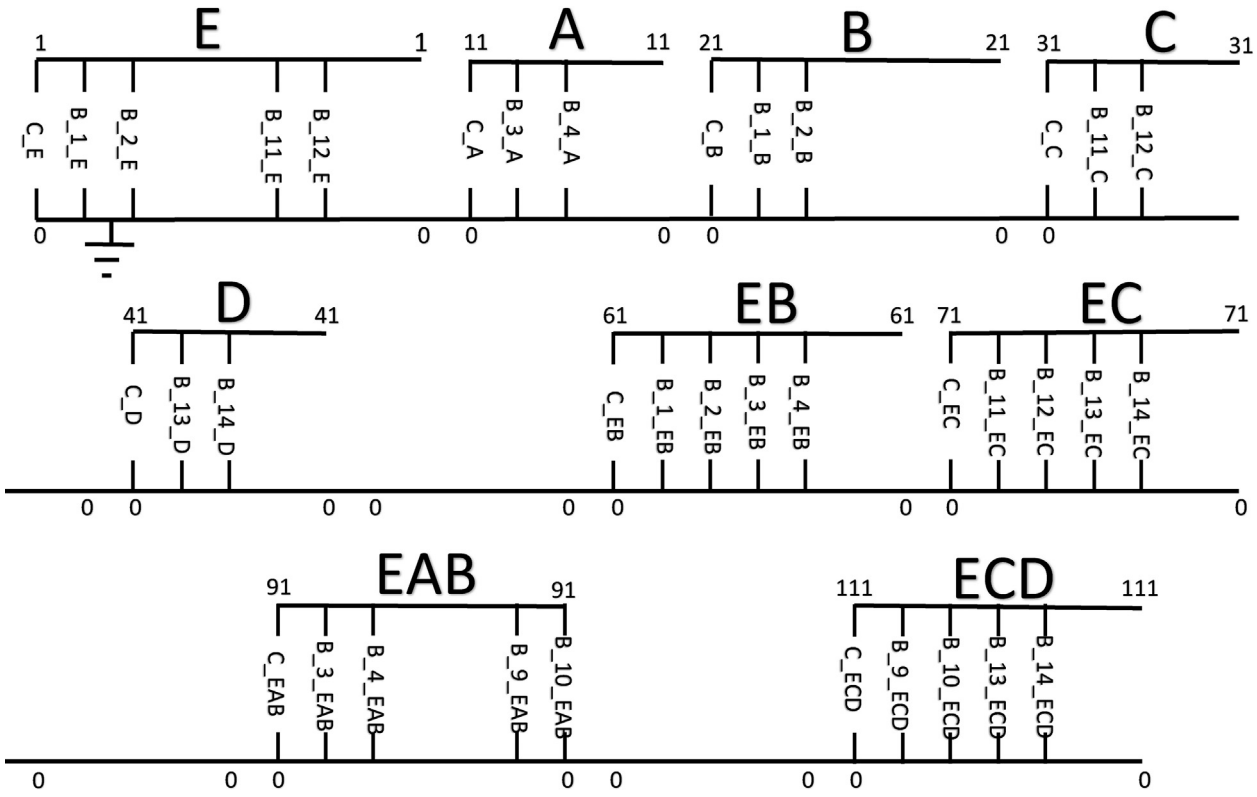

Fig. 9. Equivalent electrical network for mechanism m_6 given by the following scheme of elementary reactions: $E + B \rightleftharpoons EB; EB + A \rightleftharpoons EAB; EAB \rightleftharpoons ECD; ECD \rightleftharpoons D + EC; EC \rightleftharpoons E + C$.

which produce a net forward (positive) steady-state reaction rate or flux of the overall reaction given by Equation (9), link or couple them to an equivalent circuit, and then evaluate the steady-state flux or current by our equivalent circuit approach for each sub-cycle.

The above graph theoretical approach is illustrated for the dihydrofolate reductase network (Fig. 5). The complex pyramidal network is now seen to reduce to a simplified system containing only *seven* sub-cycles that lead to a net positive steady-state flux. The graphs of these constituent sub-cycles of the network of Fig. 5 are depicted in Fig. 8. Each of the graphs can be identified with a direct mechanism, m_1 to m_7 (Fig. 8) that makes a contribution to the net steady-state reaction rate of the pathway. The equivalent electrical network for one of these mechanisms (m_6) is shown in Fig. 9. Circuits for other mechanisms can be similarly represented, analyzed, their dynamics modeled, and their steady-state rates evaluated as shown for the complete network of the dihydrofolate reductase system in Fig. 6 and Fig. 7. The results of this computation are tabulated in Table 4. In this calculation we have essentially followed the prescription of Benkovic and Hammes-Schiffer (2003) made in their influential review in *Science* with respect to the rate constants of the DHFR reactions. The determined kinetic parameters in the pH-independent scheme for DHFR catalysis at 25 °C tabulated in Table 2 were concluded therein to "provide a basis set for examining the kinetic properties of the enzyme" (Benkovic and Hammes-Schiffer, 2003; Nath, 2022).

It ought to be stressed that no simplifying assumptions such as use of the quasi-steady-state/Bodenstein approximation or the absence of nonlinear kinetic steps in the intermediates have been made in the network and its simulation (Figs. 6 and 7). The system models mass-action kinetics of arbitrary order, and can be modified to implement other types of rate laws. We would also like to emphasize that no approximations are inherent in the process of identification of the complete finite set of sub-cycles that yield a positive net flux/current (m_1 to m_7 in this case, see Fig. 8) by our graph-theoretical approach. The present approach offers an elegant visualization of the network that is amenable to the application of powerful theorems in mathematical graph theory for abstracting other new and useful network properties (Koutrouli et al., 2020). These advantages are not available in conventional approaches that solve differential equations associated with sets of chemical reactions.

The number of sets of mechanisms and their relative contribution to the total steady state flux in the wild-type *Escherichia coli* dihydrofolate reductase pathway (Table 4) can now be readily analyzed for *maximum* steady-state flux. We expect that the path/-paths of least resistance that produce the maximum steady-state flux are the most probable mechanism(s) selected by the enzyme. The results of Table 4 show that three mechanisms, i.e. m_2, m_3, and m_6 are responsible for > 97.5 % of the total steady-state flux. The dominance of these three pathways was also noted in the original experimental work (Fierke et al., 1987). However, mechanisms m_3

Table 4
Contribution of the various direct mechanisms m_1 - m_7 to the overall steady-state reaction rate/total steady-state flux of the *Escherichia coli* dihydrofolate pathway using the kinetic parameters tabulated in Table 2.

Mechanism	Steady-state rate/flux ($\mu M\ s^{-1}$)	% contribution
m_1	0.007	0.41
m_2	0.280	16.46
m_3	0.690	40.57
m_4	0.001	0.06
m_5	0.017	0.99
m_6	0.690	40.57
m_7	0.016	0.94

and m_6 are the most likely candidates that contribute equally to the net steady-state reaction flux, at least for the wild-type *Escherichia coli* dihydrofolate reductase system (Table 4), within the modeling framework of *linearized* kinetics.

Careful observation reveals that mechanisms m_3 and m_6 are closely related to each other. Mechanism m_3 cycles sequentially through five distinct kinetic intermediate states, i.e. the holoenzyme [*EB*], Michaelis-Menten complex [*EAB*], ternary product complex [*ECD*], tetrahydrofolate binary complex [*EC*], and the tetrahydrofolate-NADPH complex [*EBC*], and back to the holoenzyme [*EB*]. Mechanism m_6 lacks the tetrahydrofolate-NADPH complex [*EBC*]; further it incorporates the apoenzyme [*E*] as the fifth intermediate. The choice between mechanism m_3 and mechanism m_6 is thus based on a razor's edge; it may well depend on cellular conditions of substrate and cofactor concentrations. A clear distinction between the two mechanisms lies in the use of the holoenzyme versus the apoenzyme. Additional information available subsequently using kinetic and structural techniques also aid us to distinguish between the two mechanisms. Since the holoenzyme is known to be biochemically active, and the intermediate state of the tetrahydrofolate-NADPH complex [*EBC*] has been detected by stopped-flow fluorescence techniques and its structure solved by X-ray crystallography (Sawaya and Kraut, 1997), mechanism m_3 may be considered the most likely mechanism for the wild-type bacterial dihydrofolate reductase system. Future work could attempt to incorporate such high-resolution structural insights into the equivalent electrical network representation by modulating the values of the circuit parameters and/or by including additional circuit elements.

In any case, it has been demonstrated here through a fairly detailed treatment of the chemical reactions of the dihydrofolate reductase system how the use of novel representation, visualization, analysis, and simulation techniques can help us, in conjunction with experimental data, in deducing the kinetics and mechanism of a complex cyclic reaction network.

6. Conclusions

The universal enzyme dihydrofolate reductase has continued to draw the attention of biological scientists and engineers, given its importance in the design of anti-folate drugs directed against tumors, pathogenic bacteria, and malarial parasites (Hitchings, 1989). A model describing the dynamics of the four-node pyramidal dihydrofolate reductase reaction network is developed. The model essentially transforms the complex cyclic reaction network into an equivalent electrical circuit analog, which is then simulated to quantify the system dynamics. A major conclusion is that a systematic reduction of the dihydrofolate network to a small set of graphs with positive net flux/reaction rate is possible. This procedure is shown to help elucidate the reaction mechanism, based on the principle of maximum flux corresponding to the path of least resistance. The developed methodology of equivalence between chemical and electrical networks is elegant, modular, fast, and has the capability to treat nonlinear reaction kinetics also, an important novel feature. The simplifying assumption of steady-state made by usual approaches to complex reaction networks – without benefit of experimental data or computer simulations – that the terminal species are always present in concentrations greatly in excess of the intermediate concentrations, and the untested approximation of linearity with respect to intermediates need to be re-evaluated to better describe bionetwork dynamics.

Uncited references

Beezer and Hansen (2012).

CRediT authorship contribution statement

Sarang S. Nath: Conceptualization, Methodology, Investigation, Formal analysis, Resources, Software, Data curation, Visualization, Writing – original draft, Writing – review & editing. **Lars K. Nielsen:** Resources, Supervision, Project administration. **John Villadsen:** Supervision.

Data availability

Data will be made available on request.

Declaration of Competing Interest

The authors declare that they have no known competing financial interests or personal relationships that could have appeared to influence the work reported in this paper.

References

Bak, T.A., Salamon, P., Andresen, B., 2002. Optimal behavior of consecutive chemical reactions. J. Phys. Chem. A 106, 10961–10964.

Beezer, A.E., Hansen, L.D., 2012. Determination of rate constants and enthalpy changes. J. Phys. Chem. B 116, 6356–6360.

Benkovic, S.J., Fierke, C.A., Naylor, A.M., 1988. Insights into enzyme function from studies on mutants of dihydrofolate reductase. Science 239 (4844), 1105–1110.

Benkovic, S.J., Hammes-Schiffer, S., 2003. A perspective on enzyme catalysis. Science 301 (5637), 1196–1202.

Blakley, R.L., 1969. In *The Biochemistry of Folic Acid and Related Pteridines* (Neuberger, A., & Tatum, E.L., Eds.), pp. 219–358. North Holland, Amsterdam.

Cellier, F.E. (Ed.), 1991. Continuous System Modeling. Springer New York, New York, NY.

Chen, T.-S., Chern, J.-M., 2003. General rate equations and their applications for cyclic reaction networks: pyramidal systems. Chem. Eng. Sci. 58 (8), 1407–1415.

Chouket, R., Pellissier-Tanon, A., Lahlou, A., Zhang, R., Kim, D., Plamont, M.-A., Zhang, M., Zhang, X.i., Xu, P., Desprat, N., Bourgeois, D., Espagne, A., Lemarchand, A., Saux, T.L., Jullien, L., 2022. Extra kinetic dimensions for label discrimination. Nat. Commun. 13 (1). https://doi.org/10.1038/s41467-022-29172-0.

Czekster, C.M., Vandemeulebroucke, A.n., Blanchard, J.S., 2011. Kinetic and chemical mechanism of the dihydrofolate reductase from *Mycobacterium tuberculosis*. Biochemistry 50 (3), 367–375.

Fierke, C.A., Johnson, K.A., Benkovic, S.J., 1987. Construction and evaluation of the kinetic scheme associated with dihydrofolate reductase from *Escherichia coli*. Biochemistry 26 (13), 4085–4092.

Fishtik, I., Callaghan, C.A., Datta, R., 2004. Reaction route graphs. examples of enzyme- and surface-catalyzed single overall reactions. J. Phys. Chem. B 108, 5683–5697.

Happel, J., Sellers, P.H., 1992. Systemization for the King–Altman–Hill diagram method in chemical kinetics. J. Phys. Chem. 96 (6), 2593–2597.

Hardiman, T., Lemuth, K., Siemann-Herzberg, M., Reuss, M., 2009. In: Dynamic modeling of the central metabolism of *E. coli* – Linking metabolite and regulatory networks. Springer, New York, pp. 209–325.

Helfferich, F.G., 2001. Kinetics of homogeneous multistep reactions. Elsevier, Amsterdam.

Hill, T.L. (Ed.), 1989. Free Energy Transduction and Biochemical Cycle Kinetics. Springer New York, New York, NY.

Hitchings, G.H., 1989. Selective inhibitors of dihydrofolate reductase (Nobel Lecture in Physiology or Medicine, 1988). In Vitro Cell and Developmental Biol. 25 (4), 303–310.

Huang, X., Wang, S., Tai, M., Zhang, L., Li, Y., 2017. Solution and computer simulation of complex linear reaction kinetics. Chem. Eng. Trans. 59, 583–588.

Juretić, D., Simunić, J., Losić, Z.B., 2019. Maximum entropy production theorem for transitions between enzyme functional states and its applications. Entropy 21, 743. https://doi.org/10.3390/e21080743.

Karlsson, E.N., Johansson, L., Holst, O., Lidén, G., 2010. *Escherichia coli* as a well-developed host for metabolic engineering. In *The Metabolic Pathway Engineering Handbook – Fundamentals* (Smolke, C.D., Ed.), Chapter 21. CRC Press, Boca Raton, FL, USA.

King, E.L., Altman, C., 1956. A schematic method of deriving the rate laws for enzyme-catalyzed reactions. J. Phys. Chem. 60 (10), 1375–1378.

Koutrouli, M., Karatzas, E., Paez-Espino, D., Pavlopoulos, G.A., 2020. A guide to conquer the biological network era using graph theory. Front. Bioeng. Biotechnol. 8, 34. https://doi.org/10.3389/fbioe.2020.00034.

Levenspiel, O., 2006. Chemical reaction engineering. John Wiley, New York.

Loveridge, E.J., Hroch, L., Hughes, R.L., Williams, T., Davies, R.L., Angelastro, A., Luk, L. Y.P., Maglia, G., Allemann, R.K., 2017. Reduction of folate by dihydrofolate reductase from *Thermotoga maritima*. Biochemistry 56 (13), 1879–1886.

Mandal, S., Sarpeshkar, R., 2009. Log-domain circuit models of chemical reactions. IEEE Int. Symposium on Circuits and Systems, 2697–2700. https://doi.org/10.1109/ISCAS.2009.5118358.

Murzin, D.Y., Avetisov, A.K., 2007. Thermodynamic consistency of complex enzymatic reactions with empty routes. Chem. Eng. Sci. 62 (22), 6492–6494.

Nath, S.S., Villadsen, J., Nielsen, L.K., 2021. Constucting equivalent electrical circuits to study the dynamics of (bio)chemical systems. Plenary Lecture, 13th ECCE–6th ECAB, DECHEMA, Berlin, September 2021.

Nath, S.S., Villadsen, J., 2022. Modeling dynamics of chemical reaction networks using electrical analogs: application to autocatalytic reactions. Chem. Eng. J. Adv. 12, 100374.

Nath, S.S., 2022. Evaluation of thermodynamic consistency of kinetic parameters in cyclic enzyme-catalyzed reaction networks. Chem. Phys. Lett. 804, 139890. https://doi.org/10.1016/j.cplett.2022.139890.

Pellissier-Tanon, A., Morgado, G., Jullien, L., Lemarchand, A., 2021. Quasi–steady–state and partial–equilibrium approximations in chemical kinetics: one stage beyond the elimination of a fast variable. ChemRxiv. https://doi.org/10.26434/chemrxiv.14198768.v2.

Poland, D., 1989. Use of Hill's cycle diagrams to obtain integrated forms for enzyme catalyzed and membrane transport reactions. J. Phys. Chem. 93 (9), 3613–3624.

Roberts, G.W., Sedra, A.S., 2010. SPICE. Oxford University Press, New Delhi.

Sawaya, M.R., Kraut, J., 1997. Loop and subdomain movements in the mechanism of *Escherichia coli* dihydrofolate reductase. Crystallographic evidence. Biochem. 36, 586–603.

Warwick, C., 2009. In a nutshell: How SPICE works. IEEE EMC Society Newsletter 22, 59–61.

Wiechert, W., 2002. Modeling and simulation: tools for metabolic engineering. J. Biotechnol. 94 (1), 37–63.